


CHEMICAL SPECIATION AND MAPPING OF THE SI IN SI DOPED LFP INGOT WITH SYNCHROTRON RADIATION TECHNIQUE

Mohammad Norouzi Banis ^{1,6}, Zhiqiang Wang,² Steeve Rousselot,³ Yulong Liu,¹ Yongfeng Hu,⁷ Majid Talebi-Esfandarani,³ Thomas Bibienne,³ Michel Gauthier,³ Ruying Li,¹ Guoxian Liang,⁵ Mickaël Dollé,³ Pierre Sauriol,⁴ Tsun-Kong Sham^{2,6*} and Xueliang Sun^{1,6*}

1. Department of Mechanical and Materials Engineering, Western University, London, ON, Canada, N6A 5B9

2. Department of Chemistry, Western University, London, ON, Canada, N6A 5B7

3. Department of Chemistry, University of Montreal, Montréal, QC, Canada, H3C 3J7

4. Department of Chemical Engineering, École Polytechnique de Montréal, Montréal, QC, Canada, H3T 1J4

5. Johnson Matthey Battery, 280 Ave. Liberté, Candiac, QC, Canada, J5R 6X1

6. Soochow-Western Centre for Synchrotron Radiation, Western University, London, ON, Canada, N6A 2B7

7. Canadian Light Source, 44 Innovation Blvd., Saskatoon, SK, Canada, S7N 2V3

Development of LiFePO₄ cathode material with high cycle life through Si doping (substituting Si at P sites of LiFePO₄) has shown that small changes to the structure of LiFePO₄ can significantly affect the performance of Li ion batteries. However, determining the nature of elemental doping and their effects on the electronic and atomic structure of LiFePO₄ remains challenging. Here we present x-ray absorption spectroscopy and x-ray fluorescence mapping as ideal characterization methods for understanding the effect of Si doped LiFePO₄ prepared using a melt-synthesis process. x-ray absorption spectra of silicon doped LiFePO₄ indicate subtle changes in the local structure surrounding the dopants compared to SiO₂ and amorphous glass phases formed as impurities in Si containing undoped samples. The study of Fe and P K-edges x-ray absorption spectra illustrates the effect of Si in the LiFePO₄ structure in doped and impurity containing samples. Utilizing x-ray absorption spectroscopy, in conjunction with x-ray fluorescence mapping, has enabled a better overview of the non-uniform nature of prepared ingot samples. These results highlight the power of x-ray absorption spectroscopy as a tool for better understanding the structure of modified LiFePO₄ and subsequently designing materials for Li ion batteries.

Keywords: Li ion battery, LiFePO₄, silicon doping, XAS, XRF mapping

INTRODUCTION

LiFePO₄ (LFP) has become a promising cathode material for lithium ion batteries. In recent years, there has been a growing demand for lithium ion batteries with larger capacity and better stability. There is also an increasing concern on safety issues regarding the use of lithium ion batteries in large-scale applications such as electric vehicles. This has led to significant research focused on addressing the challenges of LFP as a commonly used cathode material in lithium ion batteries. A primary issue with LFP is its intrinsic low electronic conductivity and lithium ion diffusion coefficient. Furthermore, there is an urgent need to improve the cycle life and long-term cyclability of LFP.^[1] Several strategies have been considered to enhance the electronic/ionic conductivity and cycle life of LiFePO₄, such as carbon coating, reduction of particle size, and element doping.^[2]

Among these research trends, element doping has the potential to significantly improve the charge/discharge property of LiFePO₄ at high current densities by enhancing lithium ion diffusion.^[3] Studies have shown that elemental doping of LFP, via solid state synthesis, can lead to favourable enhancements of the electronic and ionic conductivities of LFP.^[4] Amin et al.^[5] studied the effect of doping silicon into single crystal LFP. Their research demonstrated that compared to un-doped LFP, Si doped LFP exerted a donor effect, leading to increased ionic conductivity and lower electronic conductivity.^[5] Multi-doping was much less

frequently reported. Ban et al.,^[6] showed that co-doping of Si and F in LFP in P and O sites, respectively, could increase the electronic conductivity of LFP by 2 to 3 orders of magnitude. They attributed their result to the change in the conduction band of LFP. Nishijima et al.^[1] identified suitable elements for co-substituting at different cation sites, and that it was possible to increase the cycle life of LFP cathode. They demonstrated that the synthesized Li(Fe_{1-x}Zr_x)(P_{1-2x}Si_{2x})O₄ (x = 0.05) had a cycle life that was five times longer than pristine LFP due to reduced cell volume change upon cycling.^[1]

However, it has been shown that although Si doping of LFP in the P sites is thermodynamically possible, this process is kinetically hindered.^[7] Recently, Talebi-Esfandarani et al.^[8] reported the preparation of LFP by melt synthesis using iron ores and was left with a material composition close to that of Nishijima et al.'s: (Li_{1-z}A_z)(Fe_{1-y}M_y)(P_{1-x}Si_x)O₄. This was in close agreement with Nishijima et al.'s conclusions that the essential role of Si for the multi-doping of LFP was observed. Unravelling the nature of A and M elements and their amount in LFP was not

* Author to whom correspondence may be addressed.

E-mail address: xsun@eng.uwo.ca (X.S.); tsham@uwo.ca (T.K.S)

Can. J. Chem. Eng. 9999:1–7, 2018

© 2018 Canadian Society for Chemical Engineering

DOI 10.1002/cjce.23430

Published online in Wiley Online Library

(wileyonlinelibrary.com).

attempted, considering the numerous potential combinations owing to iron ores starting composition.

Various synthesis procedures have been studied for the synthesis of pristine and doped LFP, including solid state,^[9] sol-gel,^[10] hydrothermal,^[11] microwave,^[12] atomic layer deposition,^[13] and melt-synthesis methods.^[14] Depending on the synthesis method, different impurities are formed alongside the LFP structure, which have a significant effect on the overall performance of synthesized material. This is the case for example for impurities such as Li_3PO_4 , $\text{Li}_4\text{P}_2\text{O}_7$, and iron phosphides (Fe_xP). In addition, it has been shown that some impurities can be undetectable using x-ray diffraction techniques due to their amount, size, and/or amorphous nature. This hinders the study of doping elements using x-ray diffraction methods. Other characterization techniques such as magnetic measurements, Raman spectroscopy, and FTIR can be used to further analyze doped LFP material and some of the impurities formed during the LFP synthesis process.^[15] However, these techniques lack chemical and elemental selectivity and do not provide a clear picture of the nature of the impurities and doping elements in doped LFP. To complement these characterization techniques, x-ray absorption spectroscopy (XAS) based techniques are a viable option. XAS probes the local electronic and atomic structure of elements, providing thorough chemical and elemental sensitivity required to determine the nature of doping elements in the LFP lattice and identify possible impurities formed during the synthesis procedure. Furthermore, a combination of XAS and x-ray fluorescence (XRF) mapping, spectromicroscopy, can be used to obtain information including elemental distribution in the sample with XAS based chemical sensitivity. XAS has been extensively used to shed light on the charge/discharge mechanisms in LFP cathodes and study their structure in cell environments. There have been a few studies on the application of this technique to study the doping of LFP structures. Wang et al.^[16] used XAS to investigate the effect of molybdenum (Mo) doping in LFP structures. A study of the X-ray absorption near edge structure (XANES) spectra showed the substitution of Fe and Li ions in Mo doped LFP samples. Chiang et al.^[17] used XAS to study the effect of doping vanadium (V) into the structure of LFP. They illustrated that a detailed analysis of the extended x-ray absorption fine structure (EXAFS) region of x-ray absorption spectrum can be used to determine the location of V atoms within LFP.

Here we present results of Si doped LFP cathode materials synthesized by melt process using XAS. These findings illustrate the power of XAS in complementing other techniques in determining the nature of Si doped LFP samples and identifying impurity phases in doped LFP prepared by a melt-synthesis process.

EXPERIMENTAL PROCEDURE

The LFP samples were prepared from different iron sources for this study: iron ore concentrate (IOC) and purified iron ore concentrate (IOP) from Rio Tinto Iron Ore Company of Canada and Fe_2O_3 99+ % from Sigma-Aldrich as the purest reference precursor based on a previously reported study.^[8] The chemical compositions of the ores have been previously reported.^[8] IOC and IOP differ by Si content (4.48 % Si as SiO_2 quartz phase in IOC compared to 0.20 % in IOP). Other significant impurities for both ores are MgO and CaO in proportions close to 0.4 %. In order to understand the nature and site position of co-dopants in a Si-doped LFP structure when using IOC precursor, samples were prepared using IOP and Fe_2O_3 from Sigma-Aldrich aimed at simulating the

$(\text{Li}_{(1-z)}\text{A}_z)(\text{Fe}_{(1-y)}\text{M}_y)(\text{P}_{(1-x)}\text{Si}_x)\text{O}_4$ compositions. Since Mg and Ca are the most abundant elements in IOC besides Si, considering the size and environment of Ca^{2+} and Mg^{2+} according to Shannon and Prewitt's table,^[18,19] these elements were selected as the most likely substituent candidates. Microized SiO_2 , MgCO_3 , CaCO_3 powders from Sigma-Aldrich were used as precursors for dopants. Assuming Mg/Ca occupy Fe site whereas Si occupy P site, the stoichiometries were calculated according to $\text{Li}_x(\text{X}_y\text{Fe}_{1-y})(\text{PO}_4)_x(\text{SiO}_4)_z$ with X being either Mg or Ca.

The LFP samples were prepared using a melt-synthesis process. Details regarding this procedure have been described elsewhere.^[14]

Precise amounts of LiPO_3 made from the dehydration of LiH_2PO_4 (from TQC), Iron precursor and Fe^0 (Atomet 1001HP from Rio Tinto-QMP) and dopants were gently mixed together according to the calculated composition mentioned above and then placed in a graphite crucible. IOC and IOP is added based on its [Fe] content, whereas Fe^0 amount is used as a Fe^{3+} reducing agent. The use of LiPO_3 precursor allows the simultaneous addition of Li and P contents. However, for balancing Li and P elements, Li_2CO_3 (from FMC Lithium Co.) and $\text{NH}_4\text{H}_2\text{PO}_4$ (from Newhonte (Wuhan) Industry & Trade Co.,LTD) were used as extra sources, respectively. Some carbon black was used to avoid the oxidation of iron during synthesis. The crucibles were heated at 1100 °C for 3 h and then quenched to room temperature (25 °C) under nitrogen atmosphere to obtain ingots.

In the case of Si addition in LFP, the mixture was milled in a Spex ball mill to ensure an intimate mix simulating the distribution of Si in IOC precursor.

Detailed composition and particularities of the LFP samples examined in this study are listed in Table 1.

The ingot obtained from the synthesis was ground in a mortar with a pestle to powder below 38 μm . X-ray diffraction (XRD) was carried out on the ground powder using a Bruker D8 advance x-ray diffractometer equipped with Cu $K\alpha$ radiation source. The phase unit cells of the synthesized materials were analyzed by pattern matching program FullProf Suite.

XAS measurements were carried out at the soft x-ray micro-characterization beamline (SXRMB) at the Canadian Light Source (CLS), operating at energy range of 1.7–10 keV. XANES data was collected using bulk sensitive fluorescence yield (FLY) mode. Powdered samples were measured in a vacuum chamber end-station operating at 1.3×10^{-4} Pa. Fe, P, and Ca K-edges XAS spectra were collected using a Si (111) crystal monochromator. For low energy elements, Si and P, XANES spectra was measured using an InSb (111) crystal monochromator. XAS/XRF map collection was conducted on a microprobe end-station with a beam spot size of 10 $\mu\text{m} \times 10 \mu\text{m}$ operating at 1.3×10^{-5} Pa. This spot size was achieved using a pair of K-B mirrors for focusing purposes.^[20]

Incident beam energy was calibrated using standard SiO_2 , Fe foil, and pure LFP. The XAS spectra were background subtracted for both pre- and post-edge region and edge jump normalized to unity using the Athena software package.

RESULTS AND DISCUSSIONS

The XRD patterns of the samples are depicted in Figure 1. All samples present the diffraction peaks ascribed to the orthorhombic olivine-type structure of LiFePO_4 (*Pnma* space group- JCPDS 40–1499). Small amounts of secondary phases Li_3PO_4 or $\text{Li}_4\text{P}_2\text{O}_7$ are detected as well for all the samples. These impurities are commonly reported in molten synthesized LFP samples regardless

Table 1. Description of silicon containing LFP samples prepared by melt-synthesis process and studied by XAS

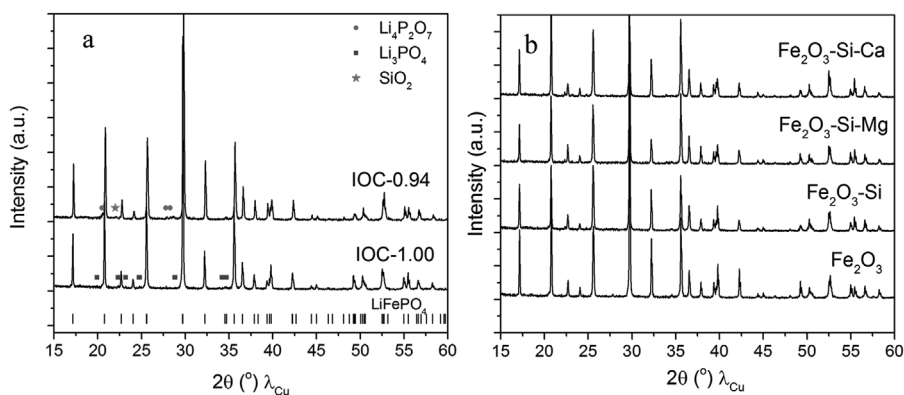
Sample Name	FeO _x Source	x Li/(Fe + Mg + Ca) & P/(Fe + Mg + Ca)	y(Mg) Mg/(Fe + Mg + Ca)	y(Ca) Ca/(Fe + Mg + Ca)	z Si/(Fe + Mg + Ca)	Description Li _x (X _y Fe _{1-y})(PO ₄) _x (SiO ₄) _z
IOC-0.94	IOC	1.067	0.004	0.005	0.046	LiPO ₃ in excess, Li, Mg, and Ca from IOC
IOC-1.00	IOC	0.997	0.004	0.005	0.046	Si, Mg, and Ca from IOC
IOP-Si	IOP	0.996	0.004	0.004	0.043	Si added as SiO ₂ ; Mg, Ca, and some Si from IOP
Fe ₂ O ₃ -Si	Fe ₂ O ₃	1.009	0.000	0.000	0.044	Si added as SiO ₂
Fe ₂ O ₃ -Si-Mg	Fe ₂ O ₃	0.969	0.020	0.000	0.021	Si added as SiO ₂ Mg added as MgCO ₃
Fe ₂ O ₃ -Si-Ca	Fe ₂ O ₃	0.969	0.000	0.020	0.021	Si added as SiO ₂ and Ca added as CaCO ₃
LFP-Si	Fe ₂ O ₃	1.009	0.000	0.000	0.044	Control sample: SiO ₂ added to LFP after melt synthesis using the same overall ratios as for the Fe ₂ O ₃ -Si sample

of the composition.^[8,14] In Figure 1a, focus is brought on the IOC-1.00 and IOC-0.94 samples. As previously reported, no extra phases related to impurity elements from IOC is visible. In contrast, a low intensity peak ascribed to SiO₂ is present in IOC-0.94. Pattern matching performed for these samples showed a slight increase of the lattice volume in IOC-1.00 compared to that of IOC-0.94. In IOC-1.00, impurity elements from IOC precursors are included in the LFP structure and, hence are not directly visible on the pattern. In contrast, no dopant is expected in the LFP structure of IOC-0.94. This is made possible via a control of the composition of the molten bath during synthesis.^[14] In IOC-1.00, on the basis solely of XRD, it is not clear whether all Si, along with other elements, is inserted in the LiFePO₄ structure or not.

Figure 1b shows the patterns for the Fe₂O₃-based samples with the addition of Si dopant only, Si + Mg and Si + Ca aiming at simulating IOC-based samples. No impurities containing Si and Mg or Ca elements can be observed in any pattern. This could mean that either these elements are all incorporated in the LFP structure, or these impurities are amorphous, and their amount is below the XRD detection limit. Considering only 0.8–1.6 wt% SiO₂ (even less for Mg and Ca) was added in each sample, this last assumption may indeed appear very likely. Refinement of the lattice parameters by pattern matching or the Rietveld method proved to be successful at evidencing doping of LFP structures. However, for very low dopant proportion and with uncertainty on the dopant amount that is inserted into the LFP structure, XRD may not be sufficiently accurate. A more direct

characterization technique such as XAS and XANES may bring valuable extra information regarding this matter.

The Si K-edge XANES spectra of silicon-containing LFP samples provide unique information pertaining to the average chemical state, local electronic, and atomic structure of Si in these samples. Figure 2 shows Si K-edge XANES spectra of two LFP samples with (a) a supposedly high percentage of Si in the LFP lattice (IOC-1.00) and (b) Si formed as an impurity phase in LFP structure (IOC-0.94). The Si K-edge XANES spectra of these samples are compared to those of amorphous and quartz SiO₂ standard samples. As shown in Figure 2a, the Si K-edge XANES spectra of the LFP samples consist of a strong whiteline at around 1847 eV. This peak is characteristic of Si⁴⁺, associated with Si 1s to 3p electronic transitions, and is aligned well with both amorphous and quartz SiO₂ XANES spectra. The origin of the shoulder peak (A) is related to the transition of Si 1s electrons to antibonding 3s-like states.^[21] For 4:2 coordinated quartz SiO₂, as shown in Figure 2b, three additional peaks are observed and denoted as B (~1851.1 eV), C (~1854.6 eV), and D (~1857.5 eV). These peaks are typically observed for well-ordered tetrahedral SiO₄ structure. Peak C is attributed to Si 1s transition to empty 3d e and t₂ states. Peaks B and D are due to multiple scattering and arise from the interaction of Si 3p states with outer-neighbouring tetrahedral orbitals, indicating long-range order.^[21,22] Standard amorphous SiO₂ displays a broad peak labelled as E following the whiteline. The IOC-0.94 sample exhibits similar features in terms of resonance shape, intensity, and position to standard amorphous SiO₂ (peak E

**Figure 1.** XRD pattern of LFP samples prepared by melt-synthesis process using different precursors.

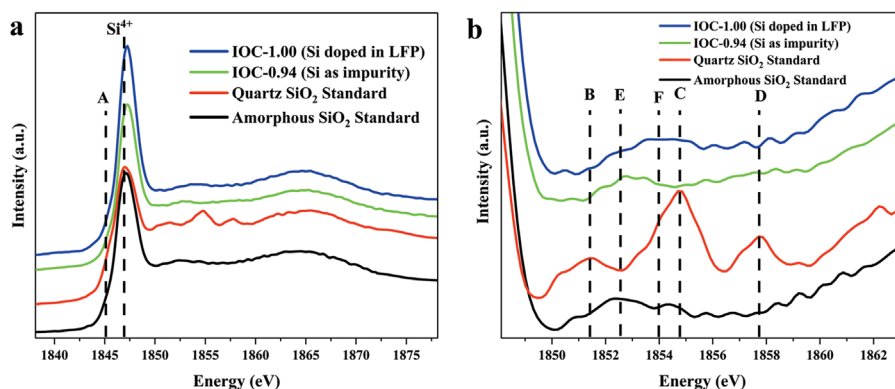


Figure 2. Si K-edge XAS spectrum of Si containing LFP samples prepared by melt-synthesis method and compared to standard SiO₂.

(~1852.5 eV)). This is a good indication that the majority of Si in the IOC-0.94 sample is in the form of amorphous SiO₂. However, the Si K-edge XANES spectrum of the IOC-1.00 sample (Figure 2b) shows a different feature (peak F (~1853.9 eV)) with respect to the peak associated with amorphous SiO₂ (peak E). This illustrates the possibility of Si existing in an alternate environment in IOC-1.00 sample compared to IOC-0.94 and standard amorphous SiO₂. This peak has been associated with cristobalite type SiO₂.^[23–24] This peak has also been observed in Si K-edge XANES spectra of silicates such as Zircon (ZrSiO₄) and Forsterite (Mg₂SiO₄), confirming the presence of Si in SiO₄ with short range order.^[21,25,26] This can be considered as an indication of a change in the location of Si in LFP (from an impurity SiO₂ base phase to a dopant in LFP structure). This confirms previous results based on XRD coupled with pattern matching refinement performed by our

group on the location of Si in LFP materials within the LFP structure or as an impurity phase.^[14]

XAS was also used to study the effect of precursors in the synthesis of Si doped LFP samples. Figure 3 shows XANES spectra of Si doped LFP samples prepared using different precursors at the Si (Figure 3a), P (Figure 3b), and Fe (Figure 3c) K-edge. The samples include the following: IOP-Si; Fe₂O₃-Si; LFP-Si (as a control sample prepared by mixing LFP with quartz SiO₂); Fe₂O₃-Si-Mg; and Fe₂O₃-Si-Ca. The Si K-edge XANES spectra of amorphous and Quartz SiO₂ were used as standards. Based on the results from Figure 2, a detailed study of the Si K-edge XANES spectra shows that the Fe₂O₃-Si sample exhibits similar features (Peak E) to amorphous SiO₂, indicating a low probability of Si doping in the LFP structure. However, IOP-Si and Fe₂O₃-Si-Mg, show characteristic features of Si as a cristobalite structure (Peak F), similar to IOC-1.00, as shown in

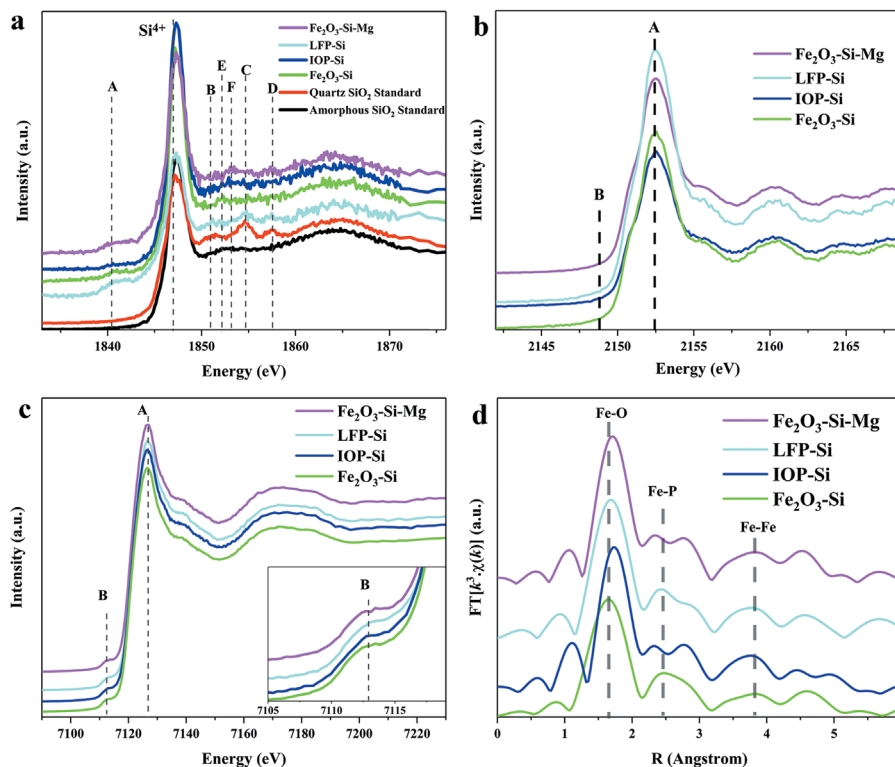


Figure 3. XAS spectra of LFP samples prepared by various source material: (a) Si K-edge; (b) P K-edge; (c) Fe K-edge; and (d) Fourier transformed k^3 weighted EXAFS of Fe K-edge spectra.

Figure 2. The higher intensity of peak F in $\text{Fe}_2\text{O}_3\text{-Si-Mg}$ compared to IOP-Si suggests that the doping percentage of Si in a critobalite phase is relatively higher for $\text{Fe}_2\text{O}_3\text{-Si-Mg}$ (with a more intense Peak F). The Si K-edge of $\text{Fe}_2\text{O}_3\text{-Si-Ca}$ (not shown here) did not illustrate any distinct features after the whiteline peak. The Si K-edge XANES spectrum of LFP-Si reveals that Si in this sample primarily exists in a quartz-like structure and aligns well with the spectra obtained for standard quartz. The Si K-edge XANES spectra of all LFP samples show a weak edge peak (A), which can be attributed to the presence of reduced Si states (lower than 4+). Slight reduction of SiO_2 could indeed be expected in the present synthesis conditions even though this mechanism appears very limited.^[27]

The P K-edge XANES spectra of synthesized LFP samples (Figure 3b) show features with PO_4^{3-} groups. The main peak (A) is assigned to transitions from 1s orbitals to unoccupied valance states with P sp^3 and O 2p characteristics.^[28,29] Studies have shown that in olivine LFP structure, during Li deintercalation, a pre-edge (B) gradually appears before the whiteline peak (A). The gradual increase in the intensity of the pre-edge peak has been associated with the hybridization of P 3p states with Fe 3d states and increasing oxidation of Fe with Li deintercalation.^[29] In the synthesized Si doped LFP samples, the absence of Peak B suggests the formation of fully lithiated LFP.

To further study the effect of precursors, Fe K-edge XANES (Figure 3c) and EXAFS spectra (Figure 3d) have been examined. In the Fe K-edge XANES spectrum of LFP samples, the pre-edge features, (Peak B) position, and the intensity of the whiteline (Peak A) provide information pertaining to the oxidation state of Fe. Pre-edge peaks represent Fe 1s to 3d transitions, which are formally dipole forbidden. However, due to mixing of Fe d-states with oxygen p-states, these transitions become possible. A weak pre-edge peak indicates the presence of Fe in an octahedral coordination (similar to LFP and $\alpha\text{-Fe}_2\text{O}_3$), while an intense pre-edge peak is a sign of tetrahedral coordination around Fe (similar to FePO_4).^[30]

According to the Fe K-edge XANES spectra (Figure 3c), all LFP samples exhibit similar XANES features, with minimal change in the whiteline intensity and position, close to those from previous reports performed on pure LFP.^[30] A close inspection of the pre-edge region (inset of Figure 3c) demonstrates relatively weak

peaks, which confirms the octahedral symmetry surrounding Fe and the formation of LFP. Figure 3d displays the Fourier transforms of the k^3 -weighted EXAFS spectra of the Fe K-edge for the Si doped LFP samples. The spectra of all four samples display a main peak at shorter distances and is associated with the Fe-O bond. The other two peaks, with relatively lower intensity, are attributed to Fe-P and Fe-Fe bonds, respectively. Minor changes in the bond distances of Fe with adjacent atoms can be observed in Figure 3d, which can be related to distortions caused by Si doping in the LFP lattice. In particular, no Fe environment related to Fe^{3+} oxidation state or in M1 site is observed in any of the samples, which is in agreement with previous results from Mössbauer analysis.^[14] Complementary analysis is required to fully understand the effect of Si on the structure of atoms surrounding Fe.

Information obtained using XAS from powdered Si-doped LFP represent an average of all the phases present in these samples. XAS can be combined with XRF mapping to provide detailed information on the surface chemical distribution of various samples. Using this method, it is possible to map non-uniformities via XRF mapping and identify possible impurity phases by XAS. To obtain a more detailed representation of non-uniformities and impurities in LFP samples prepared by melt-synthesis, the ingot samples, prior to particle size reduction, were investigated using XAS/XRF mapping technique.

Figures 4 and 5 illustrate the Fe and P XRF maps (recorded using the 7200 eV photon energy with a resolution of $\sim 10\ \mu\text{m}$) of the IOC-1.00 sample along with maps of Si as a doping agent and Ca as impurity from the precursor. These maps clearly demonstrate the non-uniform nature of LFP ingot samples. Based on the concentration of Fe, P, and Ca elements, two unique regions of the IOC-1.00 samples (relatively higher percentage of Si in LFP structure) are selected for micro-XANES analyses. The first region contains both Fe and P, with very low concentration of Ca, which is the majority phase (blue region in Figure 4a). Based on bulk Fe and P K-edge XANES spectra (Figure 3), this phase is mainly composed of LFP. The second region has a high concentration of P and Ca with a low amount of Fe. Ca K-edge XANES spectra (Figure 4b) in both regions closely resemble those of a Ca containing glass such as CaSiO_3 and Anorthite ($\text{CaAl}_2\text{Si}_2\text{O}_8$), where the pre-edge peak (C) corresponds to Ca 1s to 3d electron

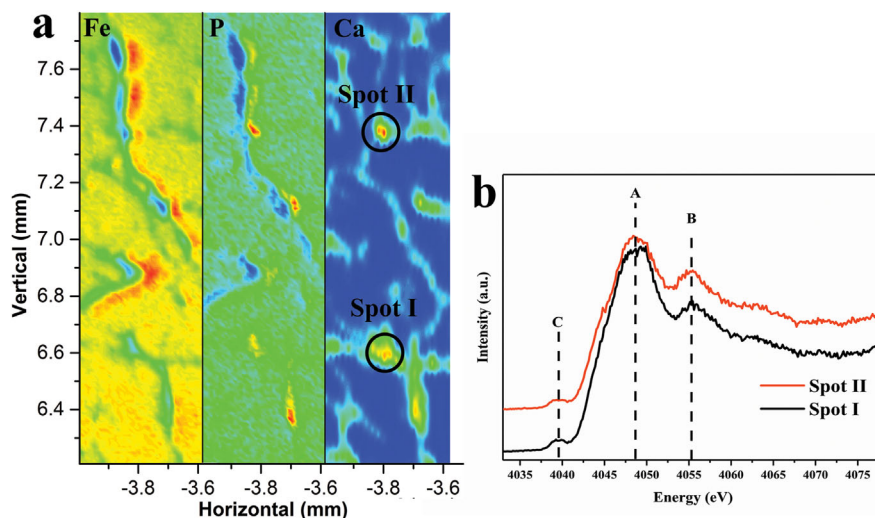


Figure 4. (a) Fe, P, and Ca XRF maps of IOC-1.00 samples; and (b) Ca K-edge XANES spectra of two impurity phases in the ingot sample.

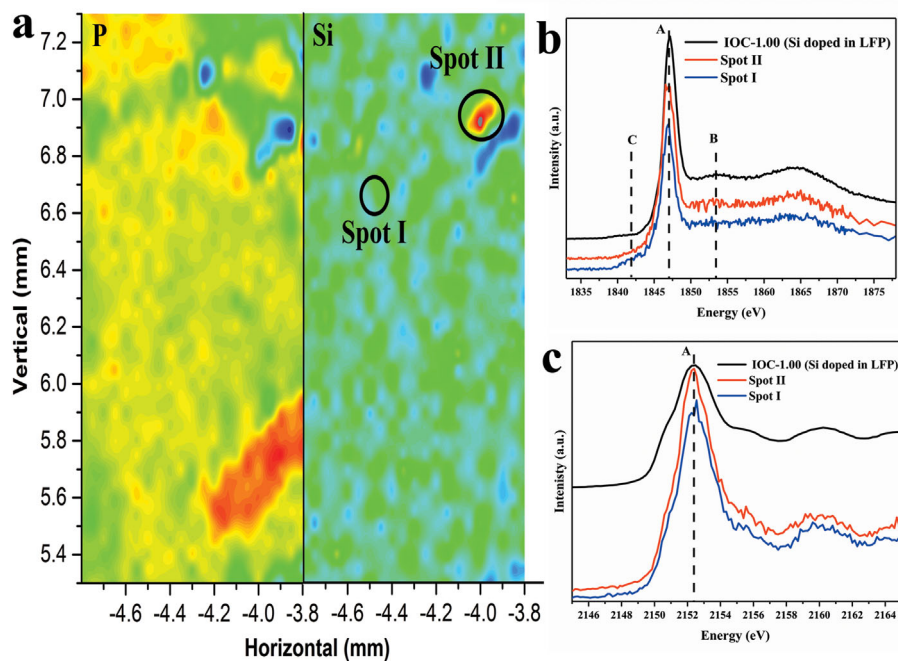


Figure 5. (a) P and Si XRF map of IOC-1.00 ingot sample; (b) Si K-edge; and (c) P K-edge XANES spectra of two spots on the ingot sample.

transitions while the main peak (A) is attributed to 1s to 3p transitions.^[31,32] It has been shown that pre-edge intensity has an inverse correlation with the local ordering and symmetry around Ca sites.^[32] A qualitative comparison between the collected data (Figure 4b) and reported studies on anorthite indicates a relatively high degree of disorder in the impurity phases observed for IOC-1.00 samples. The P and Fe K-edge XANES spectra in this region show similar features to spectra collected on the LFP phase, illustrating the smaller thickness of the impurity phase compared to the probing depth of FLY based XAS measurements.

Figure 5 shows Si and P XRF maps collected for the IOC-1.00 ingot sample using a photon energy of 2 200 eV. As seen in Figure 5a, the Si and P maps show non-uniform distribution of elements at the 10 micron-scale in this ingot sample. Theoretically, Si doping in LFP lattice can be achieved by Si substitution of P sites, thus P and Si XRF maps should show high correlation. The discrepancy is due to the presence of impurities in the form of Li_3PO_4 (using XRD characterization) and silicon-containing glasses (formed during the melt-synthesis process) and has been previously reported. Si K-edge XANES spectra (Figure 5b) regions with low (Spot I) and high (Spot II) Si concentration have been compared to IOC-1.00 powdered sample. In both regions, the whiteline position (Peak A) aligns well with the powdered sample. The Si K-edge XANES spectrum of Spot II, where there is a high Si concentration, shows a clear cristobalite characteristic peak. However, there is no indication of cristobalite structure in Spot I. A comparison of the pre-edge peak C attributed to $\text{Si}^{x<4+}$ presents a higher intensity in Spot I compared to Spot II, indicating the presence of Si as an impurity in the LFP structure. P K-edge XANES spectra (Figure 5c) in these two regions show similar features to the Si-doped in LFP powdered samples, confirming the dominant presence of LFP as main constituent.

These results illustrate the need for a detailed study of LFP samples using a combination of XAS and XRF mapping to have a clear picture of this novel cathode material synthesized for Li ion batteries.

CONCLUSION

The application of XAS has been demonstrated in studying Si doped LiFePO_4 (LFP) samples. Si K-edge XANES spectra of Si containing LFP samples provide unique information on the chemical state of Si and its local electronic and atomic structure in LFP. Using Si K-edge XANES, it is possible to differentiate between Si as an impurity phase and doping agent residing in a cristobalite type structure in LFP. These results have enabled the detailed study of Si doping in LFP material prepared using a combination of starting material (including low cost material such as ore concentrates) prepared using a melt-synthesis process. XAS results have illustrated the formation of Si-doped LFP using LFP, SiO_2 , and MgCO_3 as precursors. It has been shown that without the addition of Mg, Si forms quartz type impurities in LFP. XAS/XRF results on Si-doped LFP ingot samples have demonstrated the non-uniform distribution of impurity phases in LFP ingot sample. The formation of Ca containing glass type in ingot samples have been confirmed using XRF mapping and Ca K-edge XAS measurements. These data have highlighted the unique capabilities of XAS characterization method in studying the LFP as a cathode material in lithium ion batteries. Further theoretical modelling and experimental studies are needed to complement the data acquired from XAS measurements and provide a clear picture of chemical state and structure of doped LFP cathode material. In particular, it is not clear at this point how much Si can be inserted in the structure and the location of Mg element in the M1 or M2 site.

ACKNOWLEDGEMENTS

The authors are grateful for the support of the Natural Science and Engineering Research Council of Canada (Automotive Partnership Canada program), the Canada Light Source at University of Saskatchewan (CLS), our industrial partner Johnson-Matthey Battery Materials, and Western University. M. N. Banis and Z. Wang are grateful for the travel support award from Canadian Light Source.

REFERENCES

- [1] M. Nishijima, T. Ootani, Y. Kamimura, T. Sueki, S. Esaki, S. Murai, K. Fujita, K. Tanaka, K. Ohira, Y. Koyama, I. Tanaka, *Nat. Commun.* **2014**, *5*, 4553.
- [2] Z. Xu, L. Gao, Y. Liu, L. Li, *J. Electrochem. Soc.* **2016**, *163*, A2600.
- [3] J. Wang, X. Sun, *Energ. Environ. Sci.* **2015**, *8*, 1110.
- [4] J.-W. Zhao, S.-X. Zhao, X. Wu, H.-M. Cheng, C.-W. Nan, *J. Alloy. Compd.* **2017**, *699*, 849.
- [5] R. Amin, C. Lin, J. Peng, K. Weichert, T. Acartürk, U. Starke, J. Maier, *Adv. Funct. Mater.* **2009**, *19*, 1697.
- [6] C. Ban, W.-J. Yin, H. Tang, S.-H. Wei, Y. Yan, A. C. Dillon, *Adv. Energy Mater.* **2012**, *2*, 1028.
- [7] K. Hoang, M. D. Johannes, *J. Power Sources* **2012**, *206*, 274.
- [8] M. Talebi-Esfandarani, S. Rousselot, M. Gauthier, P. Sauriol, G. Liang, M. Dollé, *J. Solid State Electr.* **2016**, *20*, 1821.
- [9] D.-K. Kim, H.-M. Park, S.-J. Jung, Y. U. Jeong, J.-H. Lee, J.-J. Kim, *J. Power Sources* **2006**, *159*, 237.
- [10] Z. Gong, Y. Yang, *Energ. Environ. Sci.* **2011**, *4*, 3223.
- [11] S. Yang, P. Y. Zavalij, M. Stanley Whittingham, *Electrochem. Commun.* **2001**, *3*, 505.
- [12] A. V. Murugan, T. Muraliganth, A. Manthiram, *J. Phys. Chem. C* **2008**, *112*, 14665.
- [13] J. Liu, M. N. Banis, Q. Sun, A. Lushington, R. Y. Li, T. K. Sham, X. L. Sun, *Adv. Mater.* **2014**, *26*, 6472.
- [14] M. Talebi-Esfandarani, S. Rousselot, M. Gauthier, P. Sauriol, M. Duttine, A. Wattiaux, Y. Liu, X. Sun, G. Liang, M. Dollé, *J. Solid State Electr.* **2016**, *20*, 3481.
- [15] D. Jugović, D. Uskoković, *J. Power Sources* **2009**, *190*, 538.
- [16] Z. L. Wang, S. R. Sun, D. G. Xia, W. S. Chu, S. Zhang, Z. Y. Wu, *J. Phys. Chem. C* **2008**, *112*, 17450.
- [17] C. Y. Chiang, H. C. Su, P. J. Wu, H. J. Liu, C. W. Hu, N. Sharma, V. K. Peterson, H. W. Hsieh, Y. F. Lin, W. C. Chou, C. H. Lee, J. F. Lee, B. Y. Shew, *J. Phys. Chem. C* **2012**, *116*, 24424.
- [18] R. D. Shannon, C. T. Prewitt, *Acta Crystallogr. B* **1969**, *25*, 925.
- [19] R. Shannon, *Acta Crystallogr. A* **1976**, *32*, 751.
- [20] Q. F. Xiao, A. MacLennan, Y. F. Hu, M. Hackett, P. Leinweber, T. K. Sham, *J. Synchrotron Radiat.* **2017**, *24*, 333.
- [21] D. Li, G. M. Bancroft, M. E. Fleet, X. H. Feng, *Phys. Chem. Miner.* **1995**, *22*, 115.
- [22] Z. Y. Wu, F. Jollet, F. Seifert, *J. Phys.-Condens. Mat.* **1998**, *10*, 8083.
- [23] D. Li, G. M. Bancroft, M. Kasrai, M. E. Fleet, R. A. Secco, X. H. Feng, K. H. Tan, B. X. Yang, *Am. Mineral.* **1994**, *79*, 622.
- [24] N. Kamijo, K. Handa, N. Umesaki, *Mater. T. Jim.* **1996**, *37*, 927.
- [25] Z. Y. Wu, F. Seifert, *Solid State Commun.* **1996**, *99*, 773.
- [26] B. Gilbert, B. H. Frazer, F. Naab, J. Fournelle, J. W. Valley, G. De Stasio, *Am. Mineral.* **2003**, *88*, 763.
- [27] H.-C. Lee, S. Dhage, M. S. Akhtar, D. H. Kwak, W. J. Lee, C.-Y. Kim, O. B. Yang, *Curr. Appl. Phys.* **2010**, *10*, S218.
- [28] D. N. Wang, H. X. Wang, J. L. Yang, J. G. Zhou, Y. F. Hu, Q. F. Xiao, H. T. Fang, T. K. Sham, *J. Power Sources* **2016**, *302*, 223.
- [29] W. S. Yoon, K. Y. Chung, J. McBreen, K. Zaghib, X. Q. Yang, *Electrochem. Solid St.* **2006**, *9*, A415.
- [30] A. Deb, U. Bergmann, E. J. Cairns, S. P. Cramer, *J. Phys. Chem. B* **2004**, *108*, 7046.
- [31] A. Li, D. Wang, J. Xiang, R. J. Newport, M. X. Reinholdt, P. H. Mutin, D. Vantelon, C. Bonhomme, M. E. Smith, D. Laurencin, D. Qiu, *J. Non-Cryst. Solids* **2011**, *357*, 3548.
- [32] D. R. Neuville, L. Cormier, A. M. Flank, V. Briois, D. Massiot, *Chem. Geol.* **2004**, *213*, 153.

Manuscript received May 1, 2018; revised manuscript received July 12, 2018; accepted for publication July 16, 2018.